Hakula, Harri

Adaptive reference elements via harmonic extensions and associated inner modes

Published in:
Computers and Mathematics with Applications

DOI:
10.1016/j.camwa.2020.07.019

Published: 01/12/2020

Document Version
Peer-reviewed accepted author manuscript, also known as Final accepted manuscript or Post-print

ARTICLE IN PRESS

Computers and Mathematics with Applications xxx (xxxx) xxx

Contents lists available at ScienceDirect

Computers and Mathematics with Applications

journal homepage: www.elsevier.com/locate/camwa

Adaptive reference elements via harmonic extensions and associated inner modes

Harri Hakula

Aalto University, Department of Mathematics and System Analysis, P.O. Box 11100, FI–00076 Aalto, Finland

ARTICLE INFO

Article history:
Available online xxxx

Keywords:
Finite element method
p-version
Harmonic extensions
Adaptivity

ABSTRACT

A non-intrusive extension to the standard *p*-version of the finite element method is proposed. Meshes with hanging nodes are handled by adapting the reference elements so that the resulting discretisation is always conforming. The shape functions on these adaptive reference elements are not polynomials, but either harmonic extensions of the boundary restrictions of the standard shape functions or solutions to a local Poisson problem. The numerical experiments are taken from computational function theory and the efficiency of the proposed extension resulting in exponential convergence in the quantities of interest is demonstrated.

1. Introduction

Error estimation and adaptivity are hallmarks of modern numerical partial differential equation (PDE) solvers. Recently there has been a lot of interest in variations of the standard methods such as the finite element method (FEM) that address these features in some new and innovative ways. In many problems there are natural discretisations of the computational domain and it is reasonable to ask whether for instance polygonal elements could be used instead of triangles or quadrilaterals in two-dimensional problems. This immediately leads to problem of selecting the correct basis functions. Until now the shape functions have been given, what has changed is that in the new formulations the shape functions are defined computationally as solutions to some other problems, or indeed, are virtual in a well-defined way. One of the immediate benefits of such approaches is that mesh refinement can be done in a non-confirming way and thus very strong mesh gradings become simpler to implement. Arguably the virtual element method (VEM) has received the most attention with already a significant body of literature [1]. For our discussion here, the most relevant related methods are those with Trefftz-like basis functions [2,3].

With new methods comes the requirement to invest in new software infrastructure, however. In this work the fundamental objective is to preserve the existing solvers and extend the standard *p*- and *hp*-FEM solvers [4,5], in a way that lowers the threshold for implementation as much as possible, that is, non-intrusively. Hence, the goal is to implement *computable shape functions* which are compatible with the standard high order shape functions yet enable modern mesh grading within the reference element framework. The basic idea is simple: The elements can be defined with arbitrary number of points as long as the reference element mapping can be defined. In the standard formulation the nodes that do not define the mapping are called hanging nodes. Within the framework presented here there are no hanging nodes, but the space of basis functions is enriched so that every configuration results in a conforming formulation. An example is given in Fig. 1. There are three quadrilaterals with curved edges in the mesh (Fig. 1(a)) and one of them is defined with five nodes. The corresponding *adaptive reference element* or ARE for short (Fig. 1(b)) is not curved, however, since we let the standard blending function mapping take care of the curved edges. This approach differs from the ones previously proposed by Solin and Demkowicz [6,7].

E-mail address: Harri.Hakula@aalto.fi.

https://doi.org/10.1016/j.camwa.2020.07.019
0898-1221/

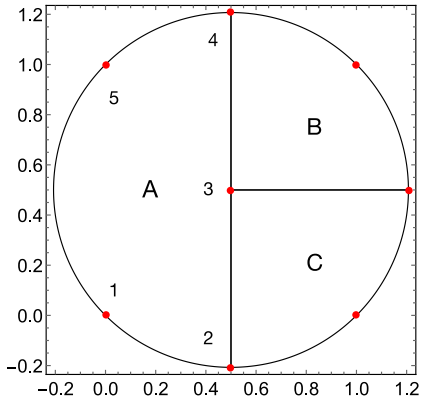

(a) Admissible mesh.

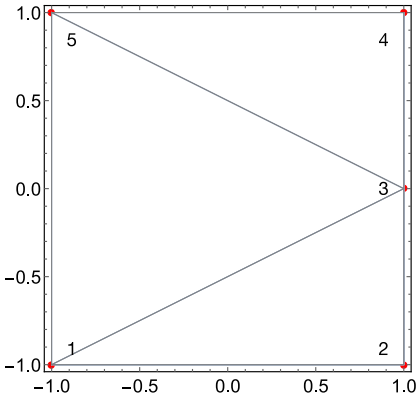

(b) One possible choice for corresponding reference element to element A.

Fig. 1. Adaptive reference element with five nodes. Minimal implementation mesh with three triangles. Curved boundaries are included in the mapping of the reference element.

The main contribution of this paper is to show that bootstrapping a FEM solver with itself is in fact, a feasible option. From a theoretical point it is interesting that the basic assumptions of the method hold automatically. In particular error estimators based on the concept of auxiliary subspaces [8] can be defined exactly as in the standard formulation. One of the difficulties inherent in practically all new approaches mentioned above is the design of quadrature rules. Our approach is not immune to these concerns. Every extension shape function is defined as a local numerical solution to some PDE. Therefore integration of any weighted inner products can always be done at the implementation level, but is more expensive. The numerical experiments do not indicate deterioration of the performance, however.

The numerical examples are motivated by computational function theory, in particular applications in electrostatics and numerical conformal mappings, classes of problems where strong singularities are often present, and hence, strong grading with efficient error estimation is necessary. In the PDE setting the construction of numerical conformal mappings requires solution of two connected Laplace problems. One of the intended applications is to be able to fit meshes, for instance in multi-capacitor problems, in a conforming way and avoid dealing with unfitted finite element methods on cut meshes as in CutFEM [9].

The rest of the paper is structured as follows: In Section 2 basic concepts on computational function theory are introduced as foundation for the numerical experiments. Also, error estimation based on the auxiliary subspaces in briefly covered; Section 3 builds on the earlier work by Weißer on boundary element based FEM [2]. The construction of the adaptive reference elements, bookkeeping, and mesh refinements are all detailed; The numerical experiments demonstrate the performance of the method, see Section 4. In all examples the p-convergence is studied with the corresponding error estimates; Finally, conclusions are discussed in Section 5.

2. Preliminaries

In this section we define concepts and algorithms used in the numerical experiments. This material is of course available in the literature but is included here to make our discussion self-contained.

2.1. Special functions

Given complex numbers a, b, and c with $c \neq 0, -1, -2, \ldots$, the *Gaussian hypergeometric function* is the analytic continuation to the slit plane $\mathbb{C} \setminus [1, \infty)$ of the series

$$F(a, b; c; z) = {}_2F_1(a, b; c; z) = \sum_{n=0}^{\infty} \frac{(a, n)(b, n)}{(c, n)} \frac{z^n}{n!}, \quad |z| < 1. \tag{1}$$

Here $(a, 0) = 1$ for $a \neq 0$, and (a, n) is the *shifted factorial function* or the *Appell symbol*

$$(a, n) = a(a + 1)(a + 2) \cdots (a + n - 1)$$

for $n \in \mathbb{N} \setminus \{0\}$, where $\mathbb{N} = \{0, 1, 2, \ldots\}$ and the *elliptic integrals* $\mathcal{K}(r), \mathcal{K}'(r)$ are defined by

$$\mathcal{K}(r) = \frac{\pi}{2} F(1/2, 1/2; 1; r^2), \qquad \mathcal{K}'(r) = \mathcal{K}(r'), \text{ and } r' = \sqrt{1 - r^2},$$

Please cite this article as: H. Hakula, Adaptive reference elements via harmonic extensions and associated inner modes, Computers and Mathematics with Applications (2020), https://doi.org/10.1016/j.camwa.2020.07.019.

which is equivalent to

$$\mathcal{K}(r) = \int_0^1 \frac{dx}{\sqrt{(1-x^2)(1-r^2x^2)}}.$$

In the following we also need the decreasing homeomorphism $\mu_a\colon (0,1) \to (0,\infty)$ defined by

$$\mu_a(r) \equiv \frac{\pi}{2\sin(\pi a)} \frac{F(a, 1-a; 1; 1-r^2)}{F(a, 1-a; 1; r^2)}. \tag{2}$$

Some basic properties of these functions can be found in [10] and [11]. The associated Dirichlet–Neumann problems are defined in (15) in Section 4.

2.2. Conformal mappings

In this section we introduce the required concepts from function theory, and present a lemma leading to a numerical algorithm. Details and proofs can be found in [12,13].

Definition 1 (*Modulus of a Quadrilateral*)**.** A Jordan domain Ω in $\mathbb{C}$ with marked (positively ordered) points $z_1, z_2, z_3, z_4 \in \partial\Omega$ is called a *quadrilateral*, and denoted by $Q = (\Omega; z_1, z_2, z_3, z_4)$. Then there is a canonical conformal map of the quadrilateral Q onto a rectangle $R_h = (\Omega'; 1+ih, ih, 0, 1)$, with the vertices corresponding, where the quantity h defines the *modulus of a quadrilateral* Q. We write

$$\mathrm{M}(Q) = h.$$

Note that the modulus h is unique.

Definition 2 (*[14, pp. 53–54], Reciprocal Identity*)**.** It is clear by the geometry that the following reciprocal identity holds:

$$\mathrm{M}(Q)\,\mathrm{M}(\tilde{Q}) = 1, \tag{3}$$

where $\tilde{Q} = (\Omega; z_2, z_3, z_4, z_1)$ is called the *conjugate quadrilateral* of Q.

Let $\gamma_j, j = 1, 2, 3, 4$ be the arcs of $\partial\Omega$ between (z_1, z_2), (z_2, z_3), (z_3, z_4), (z_4, z_1), respectively. Suppose that u_1 is the (unique) harmonic solution of the Dirichlet–Neumann problem with mixed boundary values of u_1 equal to 0 on γ_2, equal to 1 on γ_4, and $\partial u_1/\partial n = 0$ on γ_1, γ_3. Then by [14, Theorem 2.3.3]:

$$\mathrm{M}(Q) = \iint_\Omega |\nabla u_1|^2\, dx\, dy. \tag{4}$$

2.2.1. Modulus of a ring domain and Dirichlet integrals

Let E and F be two disjoint compact sets in the extended complex plane $\mathbb{C}_\infty$. Then one of the sets E, F is bounded and without loss of generality we may assume that it is E. If both E and F are connected and the set $R = \mathbb{C}_\infty \setminus (E \cup F)$ is connected, then R is called a *ring domain*. In this case R is a doubly connected plane domain. The *capacity* of R is defined by

$$\mathrm{cap}R = \inf_u \int_R |\nabla u|^2\, dm,$$

where the infimum is taken over all nonnegative, piecewise differentiable functions u with compact support in $R \cup E$ such that $u = 1$ on E. It is well-known that the harmonic function on R with boundary values 1 on E and 0 on F is the unique function that minimises the above integral. In other words, the minimiser may be found by solving the Dirichlet problem for the Laplace equation in R with boundary values 1 on the bounded boundary component E and 0 on the other boundary component F. A ring domain R can be mapped conformally onto the annulus $\{z : e^{-M} < |z| < 1\}$, where $M = \mathrm{M}(R)$ is the *conformal modulus* of the ring domain R. The modulus and capacity of a ring domain are connected by the simple identity $\mathrm{M}(R) = 2\pi/\mathrm{cap}R$.

2.2.2. Conjugate function method

Suppose that Q is a quadrilateral, and u_1 is the harmonic solution of the Dirichlet–Neumann problem and let u_2 be a conjugate harmonic function of u_1 such that $u_2(\mathrm{Re}\, z_3, \mathrm{Im}\, z_3) = 0$. Then $f = u_1 + iu_2$ is an analytic function, and it maps Ω onto a rectangle R_h such that the image of the points z_1, z_2, z_3, z_4 are $1+ih, ih, 0, 1$, respectively. Furthermore by Carathéodory's theorem, f has a continuous boundary extension which maps the boundary curves $\gamma_1, \gamma_2, \gamma_3, \gamma_4$ onto the line segments $\gamma_1', \gamma_2', \gamma_3', \gamma_4'$, see Fig. 2.

Lemma 1. *Let Q be a quadrilateral with modulus h, and let u_1 be the harmonic solution of the Dirichlet–Neumann problem. Suppose that u_2 is the harmonic conjugate function of u_1, with $u_2(\mathrm{Re}\, z_3, \mathrm{Im}\, z_3) = 0$. If $\tilde{u}_1$ is the harmonic solution of the Dirichlet–Neumann problem associated with the conjugate quadrilateral $\tilde{Q}$, then $u_2 = h\tilde{u}_1$.*

Please cite this article as: H. Hakula, Adaptive reference elements via harmonic extensions and associated inner modes, Computers and Mathematics with Applications (2020), https://doi.org/10.1016/j.camwa.2020.07.019.

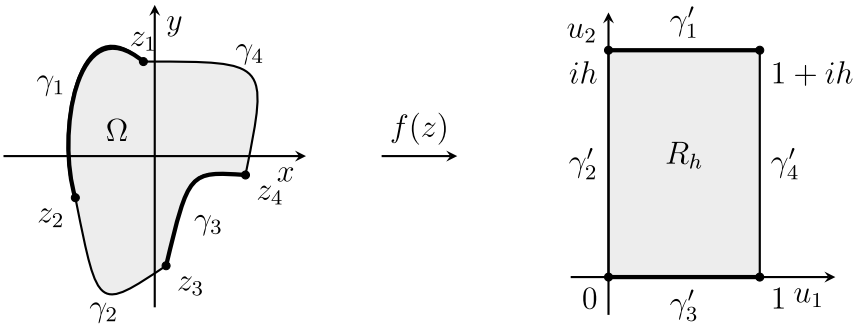

Fig. 2. Dirichlet–Neumann boundary value problem. Dirichlet and Neumann boundary conditions are marked with thin and thick lines, respectively.

Our aim is to construct a conformal mapping from a quadrilateral $Q = (\Omega; z_1, z_2, z_3, z_4)$ onto a rectangle R_h, where h is the modulus of the quadrilateral Q. Here the points z_j will be mapped onto the corners of the rectangle R_h. In the standard algorithm the required steps are the following:

Algorithm 1 (*Conformal Mapping*)**.**

1. Find a harmonic solution for a Dirichlet–Neumann problem associated with a quadrilateral.
2. Solve the Cauchy–Riemann differential equations in order to obtain an analytic function that maps our domain of interest onto a rectangle.

The Dirichlet–Neumann problem can be solved by using any suitable numerical method. One could also solve the Cauchy–Riemann equations numerically, but it is not necessary. Instead we solve u_2 directly from the conjugate problem, which is usually computationally much more efficient, because the mesh and the discretised system used in solving the potential function u_1 can be used for solving u_2 as well. This algorithm is as follows:

Algorithm 2 (*Conjugate Function Method*)**.**

1. Solve the Dirichlet–Neumann problem to obtain u_1 and compute the modulus h.
2. Solve the Dirichlet–Neumann problem associated with $\tilde{Q}$ to obtain u_2.
3. Then $f = u_1 + ihu_2$ is the conformal mapping from Q onto R_h such that the vertices (z_1, z_2, z_3, z_4) are mapped onto the corners $(1 + ih, ih, 0, 1)$.

2.3. Auxiliary subspaces

One class of methods for estimating error that has proven to be very robust in practice is the so-called hierarchical basis approach, whose origins can be traced back at least to [15]. In this approach, given a finite element approximation $\hat{u} \in V$ of the solution u, an approximate error function $\varepsilon = u - \hat{u}$ is computed in a finite dimensional auxiliary space W satisfying $V \cap W = \{0\}$. A global error estimate is obtained by measuring ε in an appropriate norm, and local norms of ε are used as local error indicators to drive an adaptive algorithm. Hierarchical basis methods belong to the broader class of implicit methods, which require the solution of additional, simpler (local or global) systems to obtain an error estimate.

Consider the abstract problem setting with $\hat{u}$as the standard piecewise polynomial finite element space on some discretisation T of the computational domain D. Assuming that the exact solution $u \in H_0^1(D)$ has finite energy, we arrive at the approximation problem: Find $\hat{u} \in V$ such that

$$a(\hat{u}, v) = l(v)\ (= a(u, v)),\ \ \forall v \in V, \tag{5}$$

where $a(\cdot, \cdot)$ and $l(\cdot)$, are the bilinear form and the load potential, respectively. Additional degrees of freedom can be introduced by enriching the space V. This is accomplished via introduction of an auxiliary subspace or "error space" $W \subset H_0^1(D)$ such that $V \cap W = \{0\}$. We can then define the error problem: Find $\varepsilon \in W$ such that

$$a(\varepsilon, v) = l(v) - a(\hat{u}, v)(= a(u - \hat{u}, v)),\ \ \forall v \in W. \tag{6}$$

In 2D the space W, that is, the additional unknowns, can be associated with element edges and interiors. Thus, for *hp*-methods this kind of error estimation is natural. The main result on this kind of estimators in H^1-seminorm (or energy) is Theorem 1.

Theorem 1 ([8])**.** *There is a constant K depending only on the dimension d, polynomial degree p, continuity and coercivity constants C and c, and the shape-regularity of the triangulation $\mathcal{T}$ such that*

$$\frac{c}{C}\|\varepsilon\|_E \le \|u - \hat{u}\|_E \le K\left(\|\varepsilon\|_E + \mathrm{osc}(R, r, \mathcal{T})\right),$$

where the residual oscillation depends on the volumetric and face residuals R and r, and the triangulation $\mathcal{T}$.

Please cite this article as: H. Hakula, Adaptive reference elements via harmonic extensions and associated inner modes, Computers and Mathematics with Applications (2020), https://doi.org/10.1016/j.camwa.2020.07.019.

The solution ε of (6) is called the *error function*. It has many useful properties for both theoretical and practical considerations. In particular, the error function can be numerically evaluated and analysed for any finite element solution. By construction, the error function is identically zero at the mesh points.

We shall use the error function is three ways below. The quantity of interest is the Dirichlet energy, i.e., the square of the H^1-seminorm. Thus, it is natural to consider $\|\varepsilon\|_E^2$ for moduli and capacities. To approximate the reciprocal error $e_r^* = |1 - \mathrm{M}(Q)\,\mathrm{M}(\tilde{Q})|$, we use the sum $\|\varepsilon_1\|_E + \|\varepsilon_2\|_E$. Finally, the effectivity index is taken to be the ratio $\|\varepsilon\|_E/E(\mathrm{M})$, where $E(\mathrm{M})$ is the square root of the exact error in the quantity of interest.

3. Construction of adaptive reference elements

In this section we discuss the formulation and implementation of the adaptive reference elements. We assume familiarity with the basic concepts of the *p*- and *hp*-versions of the finite element method [4,5]. Only 2D construction is considered. Although the 3D analogues are straightforward in principle, implementations are not. Adaptive reference elements are useful when an existing mesh is refined as in the *hp*-FEM or when the edge nodes in 2D are induced by an interface of two non-aligned meshes, for instance, in contact problems (see Fig. 1). In 3D the extension modes can be also face modes. Furthermore, the intersection of two element faces may require refinements which in turn must be conforming on both elements sharing the interface. Naturally the number of additional modes and hence added computational complexity depends on the chosen refinements. In 2D such geometric issues do not arise due to lower spatial dimension. The 2D *hp*-solver is implemented with Mathematica [16] – for the design principles, see [17].

As already alluded to in the introduction, the theoretical foundations for the method can be directly adopted from Weißer's work on boundary element based FEM [2]. Rather than repeating the arguments here, we highlight the features specific to our approach.

3.1. Definition

As usual in finite elements every element is an instance of some reference element. To fix terminology we say that every *adaptive element* (AE) is an instance of an adaptive reference element (ARE). The adaptive reference elements is defined with a set of points or nodes as usual. What is different is that a subset of nodes are used to define the mapping of the element. Let us consider the example in the introduction (Fig. 1). The mesh has three elements labelled A, B, and C. In Fig. 1(b) an adaptive reference element is shown. The quadrilateral has *five* nodes, four mapping nodes and one edge node. This choice is not unique, however. For instance, the adaptive reference element (ARE) corresponding to element A could be a triangle with mapping nodes {1,2,4} and two edge (hanging) nodes 3 and 5. Similarly, the elements B and C, could either be standard curved quadrilaterals or triangle AEs with corresponding AREs.

Definition 3 (*Planar Adaptive Reference Element (*ARE*)*)**.** Given a set of points K, $|K| \geq 3$, any partition of K into mapping and edge nodes is admissible, if the edge nodes lie on the boundary of some valid mapping of the standard reference element defined by the mapping points. This partition defines the adaptive reference element. If the set of edge nodes is empty, the adaptive reference element is equivalent to a standard element.

3.2. Shape functions

The shape functions are computed as harmonic extensions of the restrictions of the standard FEM nodal and edge functions on the element boundary. In other words, for any standard nodal or edge shape function $\phi(x, y)$ we compute its harmonic extension $\varphi(x, y)$:

$$\begin{cases} \Delta\varphi(x,y) = 0, & \text{in } \Omega, \\ \varphi(x,y) = \phi(x,y)|_{\partial\Omega}, & \text{on } \partial\Omega, \end{cases} \tag{7}$$

where Ω is either a reference quadrilateral or triangle. Some examples of such shape functions are given in Figs. 3 and 4. This construction guarantees a continuous formulation combining AEs and standard finite elements. Also notice, that the nodal modes automatically form a partition of unity.

The associated inner modes $\hat{\varphi}(x, y)$ are the functions satisfying

$$\begin{cases} \Delta\hat{\varphi}(x,y) = q(x,y), & \text{in } \Omega, \\ \hat{\varphi}(x,y) = 0, & \text{on } \partial\Omega, \end{cases} \tag{8}$$

where $q(x, y)$ is some polynomial. For instance $q(x, y) = 1$ (const) induces a standard bubble function. The set of elemental inner modes $\hat{\varphi}(x, y)_K$ is constructed with products of Legendre polynomials, that is, all $q(x, y) \in q(x, y)_K$, where

$$q(x,y)_K = \{P_i(x)P_j(y),\ i = 0,\ldots,p-2,\ j = 0,\ldots,p-2,\}.$$

With this choice the number of inner modes is the same as with the standard *p*-version, although the approximation properties are not.

Please cite this article as: H. Hakula, Adaptive reference elements via harmonic extensions and associated inner modes, Computers and Mathematics with Applications (2020), https://doi.org/10.1016/j.camwa.2020.07.019.

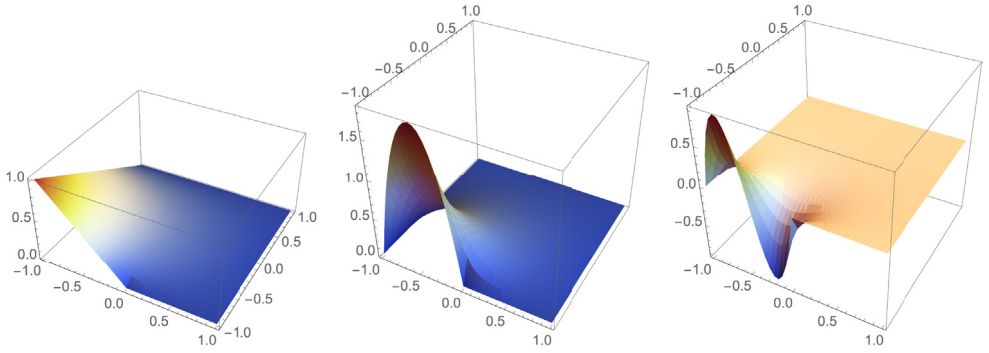

(a) Nodal mode. (b) Edge mode with $p = 2$. (c) Edge mode with $p = 3$.

Fig. 3. Quadrilateral.

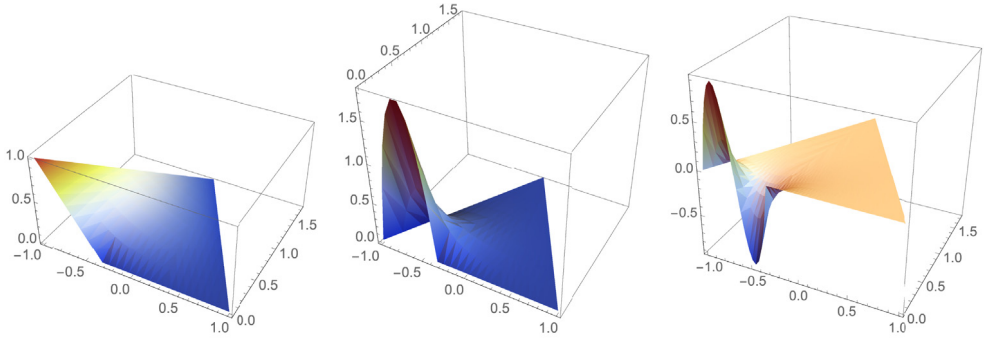

(a) Nodal mode. (b) Edge mode with $p = 2$. (c) Edge mode with $p = 3$.

Fig. 4. Triangle.

The computation of the shapes is done with finite elements (naturally!). Hence, we arrive at the concept of the *implementation mesh*, or more precisely, *implementation discretisation*. In order to simplify the evaluation of the inner products between the shape functions, we compute every shape function associated with a given element using the same implementation discretisation. One consequence of this is that the same extension may be computed using many different implementation discretisations.

For quadrilaterals our baseline implementation discretisation is a regular grid with two elements per segment and uniform $p = 20$, and for triangles a minimal triangulation of the nodes with uniform $p = 16$.

3.3. Type of reference element

In order to minimise computational work, it is necessary to introduce a way to maintain bookkeeping for the evaluated shapes and AREs. Since we want to maintain compatibility with the standard p-version, on split edges we must ensure that the shape functions have correct parities.

Legendre polynomials of degree n can be defined using a recursion formula

$$(n+1)P_{n+1}(x) - (2n+1)xP_n(x) + nP_{n-1}(x) = 0, \quad P_0(x) = 1. \tag{9}$$

For our purposes the central polynomials are the integrated Legendre polynomials for $x \in [-1, 1]$

$$\phi_n(\xi) = \sqrt{\frac{2n-1}{2}} \int_{-1}^{\xi} P_{n-1}(t)\,dt, \quad n = 2, 3, \ldots \tag{10}$$

which can be rewritten as linear combinations of Legendre polynomials

$$\phi_n(\xi) = \frac{1}{\sqrt{2(2n-1)}} \left(P_n(\xi) - P_{n-2}(\xi)\right), \quad n = 2, 3, \ldots \tag{11}$$

Please cite this article as: H. Hakula, Adaptive reference elements via harmonic extensions and associated inner modes, Computers and Mathematics with Applications (2020), https://doi.org/10.1016/j.camwa.2020.07.019.

Table 1
Summary of experiments.

Experiment	DOF ($p = 10$)	Reference
Symmetric circular quadrilateral	27681	1
Unsymmetric circular quadrilateral	27681	1.08223348626566
Grötzsch ring	34191	3.12680384539223
Planar capacitor	95301	4.133592978113

The normalising coefficients are chosen so that

$$\int_{-1}^{1} \frac{d\phi_i(\xi)}{d\xi} \frac{d\phi_j(\xi)}{d\xi}\, d\xi = \delta_{ij}, \quad i,j \geq 2. \tag{12}$$

Therefore, the $\phi_n(\xi)$ inherit the property of the Legendre polynomials,

$$\phi_n(\xi) = (-1)^n \phi_n(-\xi). \tag{13}$$

This means that every edge has to be oriented in such a way that the shape function has a consistent sign or parity on both elements sharing it.

We assign a *type* or *signature* for every element in the following way: First we choose a mapping node with the smallest identifier and rotate the simplex so that the selected node is in a fixed position (normalisation); next for each edge, the parameter range of its support on the reference element is derived; finally each edge segment is assigned a parity by comparing the identifiers of the end points. Thus every edge, split or not, has its contribution to the type of the ARE in form of a tuple $(s, [a, b])$, where $s = \pm 1$, and $-1 \leq a < b \leq 1$. For instance, the ARE of Fig. 1(b) has the type S_Q – assuming that the nodes are identified as in the picture –

$$S_Q = ((1, [-1, 1]), ((1, [-1, 0]), (1, [0, 1])), (1, [-1, 1]), (-1, [-1, 1])).$$

Here we have followed the convention that the positive direction is from the node with the smallest identifier. For standard p-version quadrilaterals there are four types, and for triangles two types. The inner modes are always assumed to be oriented in the same way, that is, they do not affect the type.

3.4. Curved elements

Since the computable shape functions are defined using finite elements, curved elements do not lead to any additional complexity. Every curved AE is mapped using the standard blending function techniques. On the implementation level this simply means that the mapping introduces scaling to quadrature weights on the ARE. We demonstrate the efficacy of this approach in the numerical examples below.

3.5. Quadrature design

As already mentioned in the introduction, the weakness of the method as currently defined is the lack of efficient quadrature rules. Obviously, for problems with constant coefficients and affine elements, the computational efficiency is the same as with standard finite elements. However, if the coefficients are not constant or the elements are not affine, the fall back quadrature rule is to use elementwise quadratures on the implementation mesh, which is expensive. One of intriguing possibilities is to use probabilistic techniques for deriving efficient *average* quadratures [18].

3.6. Mesh generation and refinement

Since the proposed method is an extension of the p-version, mesh generation is identical to that of p-version. The power of the method lies in its ability to adapt to (seemingly) non-conforming mesh refinements. In Fig. 5 two examples of strategies for refining the mesh to a corner singularity are illustrated.

The nodes are given identifiers in the order of creation. Thus, in both instances there are four AEs, but only two different types, hence, only two AREs have to be computed. Moreover, if one wanted to solve some problem using both meshes one at the time, the representative reference elements of each type would have to be computed only once. In Figs. 5(c) and 5(d) the AEs are given using nodes on edges.

4. Numerical experiments

The numerical experiments are selected from the corpus of reference problems of computational function theory and electrostatics. The first two, circular quadrilateral and Grötzsch ring are classical, and the third – also a ring problem – a planar capacitor has the salient features of real designs that make it a challenging problem. Reference data on experiments in given in Table 1.

Please cite this article as: H. Hakula, Adaptive reference elements via harmonic extensions and associated inner modes, Computers and Mathematics with Applications (2020), https://doi.org/10.1016/j.camwa.2020.07.019.

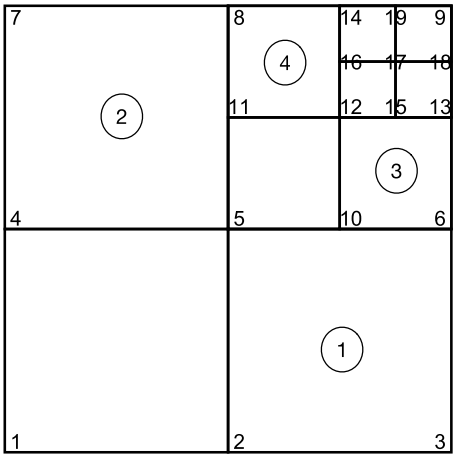

(a) Symmetric.

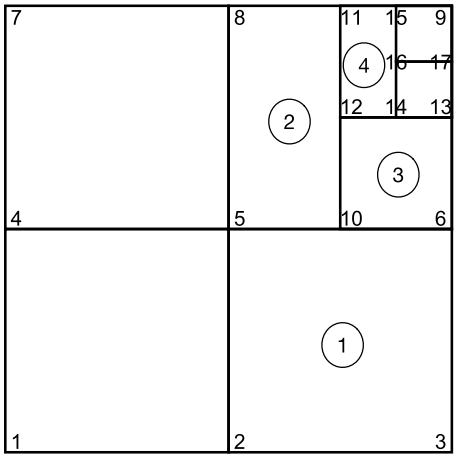

(b) Alternating.

Tag	e_1	e_2	e_3	e_4	Type
1	(2,3)	(3,6)	(6,10,5)	(5,2)	1
2	(4,5)	(5,11,8)	(8,7)	(7,4)	2
3	(6,13)	(13,15,12)	(12,10)	(10,6)	2
4	(8,11)	(11,12)	(12,16,14)	(14,8)	1

(c) Symmetric: List of AEs and AREs (types).

Tag	e_1	e_2	e_3	e_4	Type
1	(2,3)	(3,6)	(6,10,5)	(5,2)	1
2	(5,10)	(10,12,11)	(11,8)	(8,5)	2
3	(6,13)	(13,14,12)	(12,10)	(10,6)	2
4	(11,12)	(12,14)	(14,16,15)	(15,11)	1

(d) Alternating: List of AEs and AREs (types).

Fig. 5. Two examples of mesh refinement strategies. Three levels of elements towards the upper hand corner. Normalised AEs are given as node lists, every split edge has the same parametrisation on the reference element. Types are labelled in the order of occurrence.

In this section we adopt the convention that we use terms modulus and capacity interchangeably. We denote the capacity of the original problem with solution u_1 with R_1 and that of the conjugate one with R_2. Then the reciprocal error is

$$e_r^\star = |1 - R_1 R_2|.$$

For convenience we define the error order which is simply an integer that gives a measure of the quality of the solution.

Definition 4 (*Error Order*)**.** Given a reciprocal error $e_r^\star$, the positive integer e_i,

$$e_i = |\lceil \log(e_r^\star) \rceil|, \tag{14}$$

is referred to as the error order.

Since the ring problems can be recast as quadrilateral ones, this gives us one unified way to measure accuracy of the solutions.

For every problem the corresponding conformal map is found using the solutions of the original and conjugate problem pairs. The problem pairs are computed over a sequence of discretisations, where the polynomial order p is coupled with the level of symmetric refinements to singularities, $p = 2, 3, \ldots, 10$. That is, the mesh changes as the polynomial order increases in the sequence. In all cases the convergence is reported both in capacity and reciprocal error, including the error estimates based on auxiliary subspaces, where the space W is chosen to include edge modes at $p+1$ and $p+2$, and inner modes at $p-1$, unless otherwise specified.

Please cite this article as: H. Hakula, Adaptive reference elements via harmonic extensions and associated inner modes, Computers and Mathematics with Applications (2020), https://doi.org/10.1016/j.camwa.2020.07.019.

Formally, every problem is defined on some computational domain Ω, with boundary admitting a partition $\partial\Omega = \cup_{j=1}^4 \gamma_j$, where the arcs γ_j are as defined in Section 2.2. Then the problem (O) and its conjugate (C) are:

$$\text{(O)}\ \begin{cases} \Delta u_1 = 0, & \text{in } \Omega, \\ u_1 = 0, & \text{on } \gamma_1, \\ u_1 = 1, & \text{on } \gamma_3, \\ \frac{\partial u_1}{\partial n} = 0, & \text{on } \gamma_2 \text{ and } \gamma_4, \end{cases} \qquad \text{(C)}\ \begin{cases} \Delta u_2 = 0, & \text{in } \Omega, \\ u_2 = 0, & \text{on } \gamma_2, \\ u_2 = 1, & \text{on } \gamma_4, \\ \frac{\partial u_2}{\partial n} = 0, & \text{on } \gamma_1 \text{ and } \gamma_3. \end{cases} \tag{15}$$

Thus, in different cases it is sufficient to identify the boundary partition $\partial\Omega = \cup_{j=1}^4 \gamma_j$.

4.1. Circular quadrilaterals

Our first experiment concerns a family of circular quadrilaterals [12]. The absolute ratio of four points $a, b, c, d \in \mathbb{C}$ is defined as

$$|a, b, c, d| = \frac{|a-c||b-d|}{|a-b||c-d|}. \tag{16}$$

The main property of the absolute ratio is the Möbius invariance:

$$|a, b, c, d| = \big|w(a), w(b), w(c), w(d)\big|, \tag{17}$$

if w is a Möbius transformation

$$w(z) = \frac{kz+l}{mz+n}, \quad (kn - ml \neq 0). \tag{18}$$

Given z_1, z_2, z_3 on a circle (or on a line) and w_1, w_2, w_3 on a circle (or on a line), there exists a Möbius transformation w with $w(z_j) = w_j,\ j = 1, 2, 3$.

Let $0 < a < b < c < 2\pi$ and choose the points $\{1, e^{ia}, e^{ib}, e^{ic}\}$ on the unit circle with the absolute ratio

$$\big|1, e^{ia}, e^{ib}, e^{ic}\big| = \frac{\sin(b/2)\sin((c-a)/2)}{\sin(a/2)\sin((c-b)/2)} = u. \tag{19}$$

Now the unit disk, together with the boundary points $e^{ia}, e^{ib}, e^{ic}, 1$ determines a circular quadrilateral denoted by Q_B. Using an auxiliary Möbius transformation of the unit disk onto the upper half plane we can readily express the modulus using the capacity of the Teichmüller ring domain [10, Section 7] and express it as follows

$$\mathsf{M}(Q_B; e^{ia}, e^{ib}, e^{ic}, 1) = \frac{1}{2}\tau(u-1), \tag{20}$$

where u is as in (19), and

$$\tau(t) = \pi/\mu_{1/2}(1/\sqrt{1+t}), \qquad t > 0,$$

and $\mu_{1/2}(r)$ is as in (2), gives the conformal capacity of the plane Teichmüller ring.

We consider two examples of such quadrilaterals: The symmetric one

$$(Q_B; e^{i\pi/2}, e^{i\pi}, e^{i(3\pi/2)}, 1)$$

and the unsymmetric one

$$(Q_B; e^{i\pi/4}, e^{i\pi/2}, e^{i(3\pi/2)}, 1).$$

These are illustrated in Figs. 6 and 7, respectively. For the symmetric case it follows immediately from the reciprocal identity that the capacity must be equal to one. Of course, one can calculate the absolute ratio $u = 2$ and thus get $\frac{1}{2}\tau(1) = 1$.

4.1.1. hp-convergence

In Fig. 8 the *hp*-convergence graphs are shown for both circular quadrilaterals and types of error considered here: capacity and reciprocal error. Due to symmetry one would expect faster convergence in the symmetric case. This is indeed the case in terms of accuracy. It can also be seen that the auxiliary subspace construction is not p-robust at least with the standard choice of the space. In the unsymmetric case the auxiliary subspace was taken to include shapes up to $p+4$ on the edges and $p+1$ in the interior. In Figs. 8(c) and 8(d) the effect of the larger auxiliary subspace is evident. Similarly, the effectivity is higher for the larger auxiliary subspace (Fig. 9). The effectivities are comparable to those obtained in Poisson (source) problems [8]. It has to be admitted, however, that at the moment there are no theoretical results to guide us in reliable design of the auxiliary subspaces.

Please cite this article as: H. Hakula, Adaptive reference elements via harmonic extensions and associated inner modes, Computers and Mathematics with Applications (2020), https://doi.org/10.1016/j.camwa.2020.07.019.

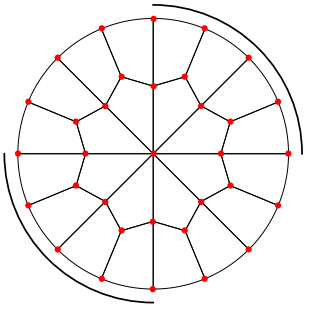

(a) Initial mesh.

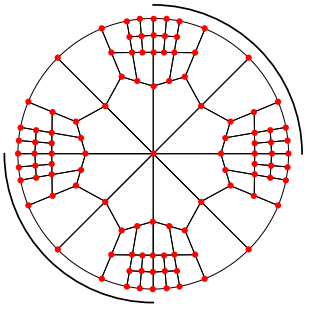

(b) Mesh with refinements.

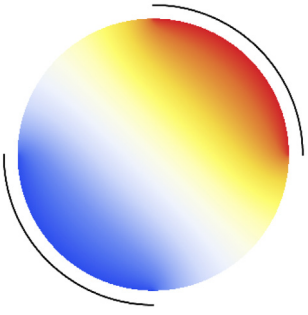

(c) Solution of the original problem u_1.

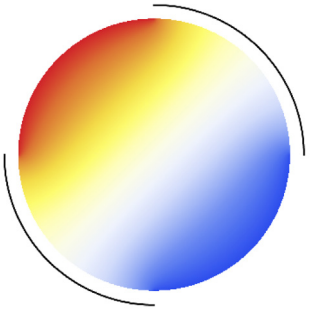

(d) Solution of the conjugate problem u_2.

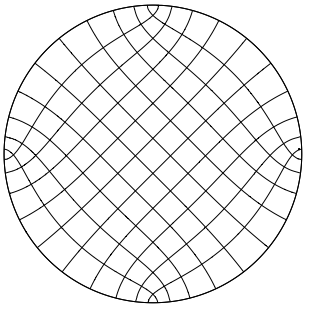

(e) Conformal map.

Fig. 6. Symmetric $(Q_B; e^{i\pi/2}, e^{i\pi}, e^{i(3\pi/2)}, 1)$. The Dirichlet sections of the original problem are indicted with a black segment. Due to symmetry, both capacities are equal to one, exactly.

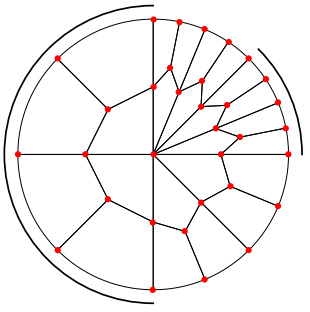

(a) Initial mesh.

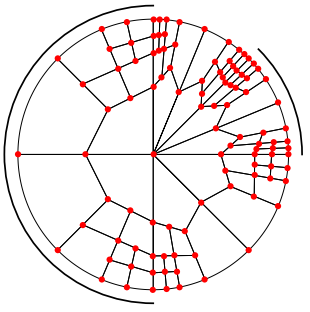

(b) Mesh with refinements.

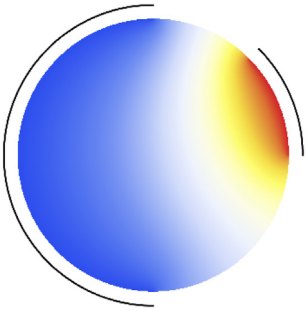

(c) Solution of the original problem u_1.

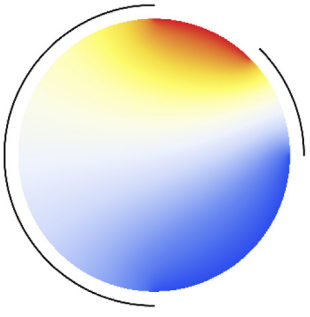

(d) Solution of the conjugate problem u_2.

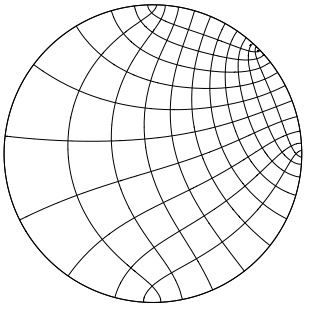

(e) Conformal map.

Fig. 7. Unsymmetric $(Q_B; e^{i\pi/4}, e^{i\pi/2}, e^{i(3\pi/2)}, 1)$. The Dirichlet sections of the original problem are indicted with a black segment.

Please cite this article as: H. Hakula, Adaptive reference elements via harmonic extensions and associated inner modes, Computers and Mathematics with Applications (2020), https://doi.org/10.1016/j.camwa.2020.07.019.

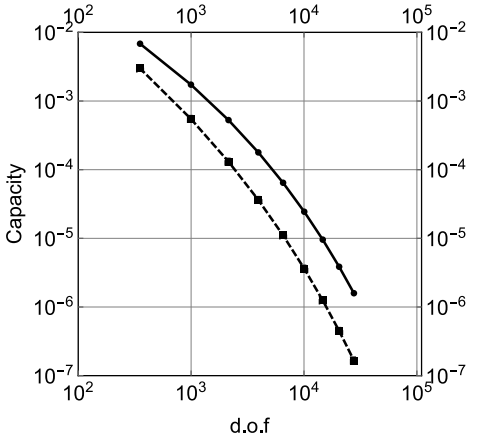

(a) $(Q_B; e^{i\pi/2}, e^{i\pi}, e^{i(3\pi/2)}, 1)$: Capacity.

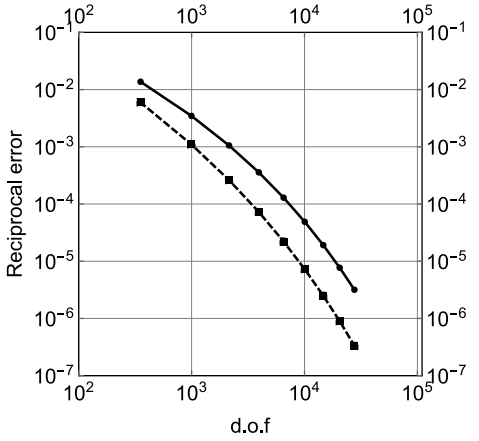

(b) $(Q_B; e^{i\pi/2}, e^{i\pi}, e^{i(3\pi/2)}, 1)$: Reciprocal error.

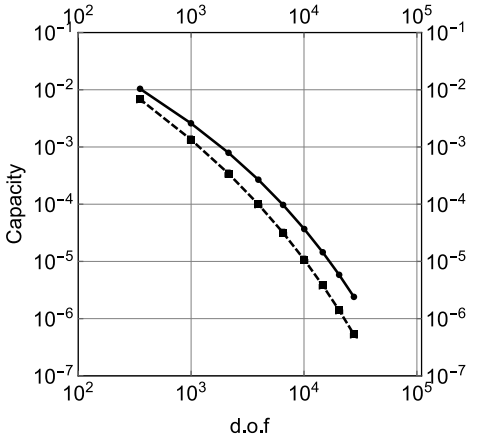

(c) $(Q_B; e^{i\pi/4}, e^{i\pi/2}, e^{i(3\pi/2)}, 1)$: Capacity.

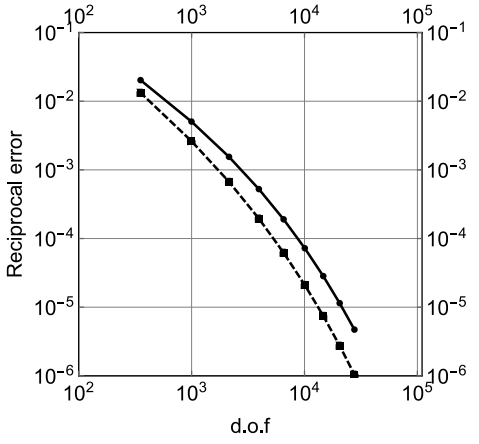

(d) $(Q_B; e^{i\pi/4}, e^{i\pi/2}, e^{i(3\pi/2)}, 1)$: Reciprocal error.

Fig. 8. Convergence of capacity and reciprocal error on two circular quadrilaterals. Exact error (solid line); Estimated error (dashed line). Loglog-plots with error vs the number of degrees of freedom. At $p = 10$ the error number = 5.

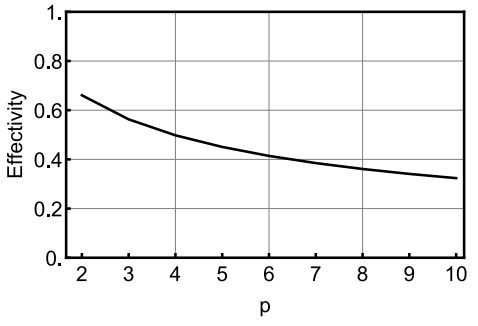

(a) $(Q_B; e^{i\pi/2}, e^{i\pi}, e^{i(3\pi/2)}, 1)$

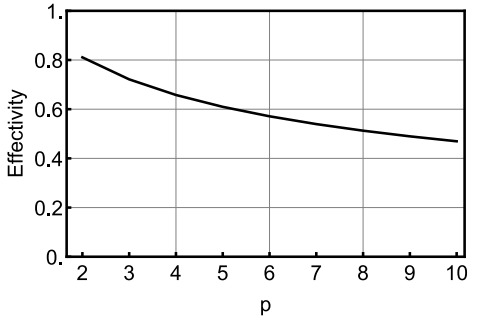

(b) $(Q_B; e^{i\pi/4}, e^{i\pi/2}, e^{i(3\pi/2)}, 1)$

Fig. 9. Effectivities of the estimated errors.

Please cite this article as: H. Hakula, Adaptive reference elements via harmonic extensions and associated inner modes, Computers and Mathematics with Applications (2020), https://doi.org/10.1016/j.camwa.2020.07.019.

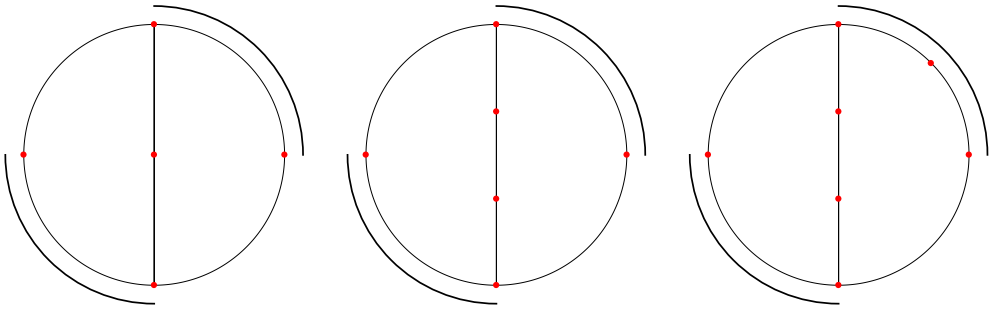

(a) T_1: One split straight edge.

(b) T_2: One straight edge split into three parts.

(c) T_3: One straight edge split into three parts and one split curved edge.

Fig. 10. Symmetric $(Q_B; e^{i\pi/2}, e^{i\pi}, e^{i(3\pi/2)}, 1)$. Two-triangle configurations.

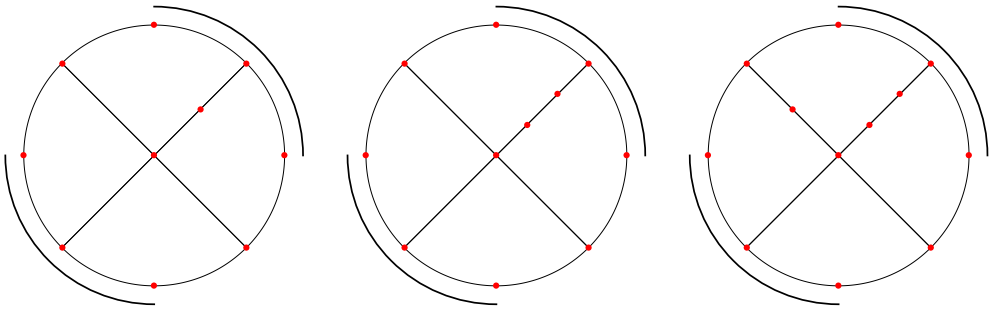

(a) Q_1: One split straight edge.

(b) Q_2: One straight edge split into three parts.

(c) Q_3: One straight edge split into three parts and another one split into two.

Fig. 11. Symmetric $(Q_B; e^{i\pi/2}, e^{i\pi}, e^{i(3\pi/2)}, 1)$. Four quadrilateral configurations.

4.1.2. Minimal configuration; Stability

Let us next study numerical stability of the methods computationally with (almost) minimal configurations with the reference solution taken from the corresponding p-version solution. In Figs. 10 and 11 two sequences of simple configurations are shown. In both cases the number of split edges, i.e., edge nodes, is increased and the complexity of the elements increases. The results are tabulated in Tables 2 and 3.

The shape function are solutions of the Laplace problem so one would expect them to be more efficient than the standard p-version integrated Legendre polynomials in this class of problems. This is, in fact, exactly what we observe. This is especially clear in the case of the two-triangle configurations. All three test cases are more accurate than the reference solution at 50 d.o.f. Moreover, as the polynomial order increases, in all cases the method converges and no numerical stalling is observed. This will be evident in the larger examples below as well.

For the quadrilateral case the reference mesh is symmetric and thus both capacity errors are too. However, the test cases are not symmetric and this is visible in the errors.

Of course, these results only indicate that the underlying implementation discretisation is sufficient for the problems considered here. One could push for higher polynomial orders or finer details in the solution mesh and eventually the implementation errors would play a significant role.

4.1.3. Timing and effect of quadrature

Let us consider the unsymmetric $(Q_B; e^{i\pi/4}, e^{i\pi/2}, e^{i(3\pi/2)}, 1)$. There are four singularities and with the symmetric refinement strategy as p increases by one, the number of AEs increases by four. Since the basis functions are hierarchic it is sufficient to compute the reference elements only at the highest value of $p = 10$. On a modern iMac Pro, with x cores and 128 MB memory, it takes 20 min to build the reference elements. Once the reference elements are available

Please cite this article as: H. Hakula, Adaptive reference elements via harmonic extensions and associated inner modes, Computers and Mathematics with Applications (2020), https://doi.org/10.1016/j.camwa.2020.07.019.

Table 2
$(Q_B; e^{i\pi/2}, e^{i\pi}, e^{i(3\pi/2)}, 1)$: Errors in two-triangle configurations. Reference configuration is a standard p-version one. DOF are given at $p = 2, 3, \ldots, 10$.

DOF	$\lvert 1-R_1\rvert$	$\lvert 1-R_2\rvert$	$\lvert 1-R_1R_2\rvert$	DOF	$\lvert 1-R_1\rvert$	$\lvert 1-R_2\rvert$	$\lvert 1-R_1R_2\rvert$
9	0.177329	0.177309	0.38608	11	0.168561	0.168561	0.365535
14	0.154538	0.154538	0.332958	17	0.146668	0.146668	0.314847
19	0.153120	0.153112	0.329677	23	0.137797	0.137797	0.294583
24	0.148808	0.14881	0.319762	29	0.133149	0.133149	0.284027
29	0.148208	0.148205	0.318379	35	0.130867	0.130867	0.27886
34	0.146575	0.146576	0.314636	41	0.128904	0.128904	0.274424
39	0.146476	0.146475	0.314407	47	0.128003	0.128003	0.27239
44	0.145794	0.145795	0.312844	53	0.126974	0.126974	0.270069
49	0.145758	0.145758	0.312761	59	0.12659	0.12659	0.269204
(a) Reference configuration				(b) T_1			
DOF	$\lvert 1-R_1\rvert$	$\lvert 1-R_2\rvert$	$\lvert 1-R_1R_2\rvert$	DOF	$\lvert 1-R_1\rvert$	$\lvert 1-R_2\rvert$	$\lvert 1-R_1R_2\rvert$
13	0.164983	0.164983	0.357185	15	0.156161	0.165028	0.346959
20	0.144921	0.144921	0.310845	23	0.140756	0.145033	0.306203
27	0.136704	0.136704	0.292096	31	0.134086	0.136763	0.289187
34	0.1324	0.1324	0.282329	39	0.130872	0.132503	0.280716
41	0.13034	0.13034	0.277668	47	0.128964	0.130411	0.276194
48	0.128491	0.128491	0.273492	55	0.127701	0.128599	0.272722
55	0.127697	0.127697	0.2717	63	0.126856	0.127782	0.270848
62	0.126719	0.126718	0.269494	71	0.126239	0.126834	0.269084
69	0.126404	0.126404	0.268786	79	0.125815	0.126502	0.268233
(c) T_2				(d) T_3			

Table 3
$(Q_B; e^{i\pi/2}, e^{i\pi}, e^{i(3\pi/2)}, 1)$: Errors in four-quadrilateral configurations. Reference configuration is a standard p-version one. DOF are given at $p = 2, 3, \ldots, 10$.

DOF	$\lvert 1-R_1\rvert$	$\lvert 1-R_2\rvert$	$\lvert 1-R_1R_2\rvert$	DOF	$\lvert 1-R_1\rvert$	$\lvert 1-R_2\rvert$	$\lvert 1-R_1R_2\rvert$
25	0.129045	0.129045	0.274742	27	0.130817	0.130272	0.27813
49	0.0850013	0.0850013	0.177228	52	0.081616	0.0814302	0.169692
81	0.057747	0.057747	0.118829	85	0.0550256	0.0549505	0.113
121	0.0430179	0.0430179	0.0878864	126	0.0413749	0.0413468	0.0844324
169	0.0341001	0.0341001	0.0693631	175	0.0331716	0.0331589	0.0674304
225	0.0281078	0.0281078	0.0570057	232	0.02755	0.0275399	0.0558487
289	0.0237785	0.0237785	0.0481224	297	0.0233899	0.023378	0.0473148
361	0.0204991	0.0204991	0.0414183	370	0.0201875	0.0201722	0.0407669
441	0.0179349	0.0179349	0.0361915	451	0.0176662	0.0176471	0.035625
(a) Reference configuration				(b) Q_1			
DOF	$\lvert 1-R_1\rvert$	$\lvert 1-R_2\rvert$	$\lvert 1-R_1R_2\rvert$	DOF	$\lvert 1-R_1\rvert$	$\lvert 1-R_2\rvert$	$\lvert 1-R_1R_2\rvert$
29	0.130824	0.130277	0.278144	31	0.131461	0.13146	0.280203
55	0.0816251	0.0814378	0.16971	58	0.0798961	0.0798956	0.166175
89	0.0550362	0.0549607	0.113022	93	0.053712	0.0537119	0.110309
131	0.0413868	0.0413583	0.0844567	136	0.0406352	0.0406348	0.0829212
181	0.0331842	0.0331709	0.0674559	187	0.0328001	0.0327994	0.0666753
239	0.0275629	0.0275519	0.0558742	246	0.0273627	0.0273615	0.0554729
305	0.0234028	0.0233894	0.0473396	313	0.0232804	0.0232785	0.0471009
379	0.0202002	0.0201828	0.0407907	388	0.0201074	0.0201047	0.0406164
461	0.0176787	0.0176568	0.0356477	471	0.017598	0.0175944	0.0355021
(c) Q_2				(d) Q_3			

the time spent in integration and assembly for 104 standard quadrilaterals and 160 AEs is 2.2 and 2.6 s, respectively. The time spent in the linear solver is 1.6 s. This ratio of time spent in integration over linear solver is typical for FEM solvers implemented in high-level languages such as Mathematica.

Notice, that the time spent in standard quadrilaterals includes construction of the elements. Nevertheless, the quadrature penalty is there but is not prohibitively large. Because of the way the element mappings are implemented, these results are representative also for problems with variable coefficients.

4.2. Grötzsch ring

Our third example is a classical ring domain, the Grötzsch ring shown in Fig. 12(a). For some historical remarks and extensions see [19]. The Grötzsch ring $R_G(r) = \mathbb{D} \setminus [0, r]$, $r \in (0, 1)$ has the capacity $\operatorname{cap}(R_G(r)) = 2\pi/\mu(r)$, were $\mu(r)$ is

Please cite this article as: H. Hakula, Adaptive reference elements via harmonic extensions and associated inner modes, Computers and Mathematics with Applications (2020), https://doi.org/10.1016/j.camwa.2020.07.019.

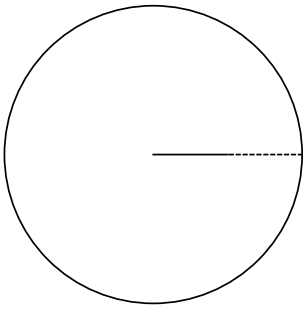

(a) Domain with cut indicated.

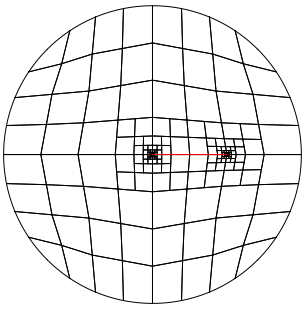

(b) Refined mesh.

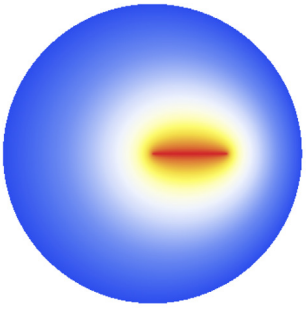

(c) Solution of the original problem u_1.

(d) Solution of the conjugate problem u_2.

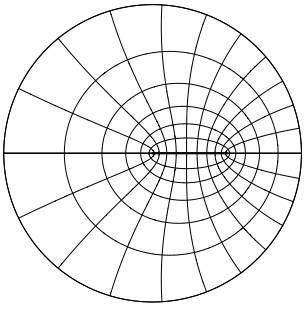

(e) Conformal map.

Fig. 12. Grötzsch Ring; $R_G(1/2)$.

the Grötzsch modulus function (cf. [10, Chapter 5]):

$$\mu(r) = \frac{\pi}{2}\frac{\mathcal{K}(r')}{\mathcal{K}(r)},$$

with usual notation $r' = \sqrt{1-r^2}$ as above.

Every ring problem can be transformed to a pair of quadrilaterals by *cutting* the domain along a path of steepest descent connecting the interior to the exterior. In this case, due to symmetry the cut can be chosen a priori without solving the ring problem first. The simple cut is indicated in Fig. 12(a) and its meaning clearly visible in Fig. 12(d). Let us formally define the boundary partition: γ_1 is the unit circle in the counterclockwise direction starting at and returning to $(1, 0)$, γ_2 is the straight line from $(1, 0) \to (1/2, 0)$, γ_3 is the interior (self-overlapping) segment $(1/2, 0) \to (0, 0) \to (1/2, 0)$, and finally γ_4 is the straight line from $(1/2, 0) \to (0, 0)$ completing the $\partial\Omega$.

The solution is dominated by the two singularities at the end points of the interior segment. The background mesh is fairly dense and the refinements are only at the singularities (Fig. 12(b)). As expected, the convergence is again exponential both in capacity and reciprocal error (see Fig. 13).

4.3. Planar capacitor

The final example is a planar capacitor design (see Fig. 14) in the spirit of a recent study of reference configurations [20]. (Notice that the term condenser is often used instead of capacitor.) In this case the exact value of the capacity is not known, but the reference result is computed up to 12 decimals using the reference solver validated in the abovementioned study.

As in the previous example the ring problem can be transformed to a pair of quadrilaterals. Again, the cut can be chosen using symmetry (Fig. 14(a)), this time the boundary curve intersects with itself four times at the centre of the cross. The mesh has been refined only at the tips of the cross.

For the sake of completeness let us formally define the boundary partition: γ_1 is the boundary of the unit square traversed counterclockwise direction starting at and returning to $(0, 1/2)$, γ_2 is the straight line from $(0, 1/2) \to (1/3, 1/2)$, γ_3 is the interior cross defined by the set of points

$$C = \{(1/3, 1/2),(1/2, 1/2), (1/2, 2/3), (1/2, 1/2), (2/3, 1/2), \\ (1/2, 1/2), (1/2, 1/3), (1/2, 1/2), (1/3, 1/2)\},$$

and finally γ_4 is the straight line from $(1/3, 1/2) \to (0, 1/2)$ completing the $\partial\Omega$.

Please cite this article as: H. Hakula, Adaptive reference elements via harmonic extensions and associated inner modes, Computers and Mathematics with Applications (2020), https://doi.org/10.1016/j.camwa.2020.07.019.

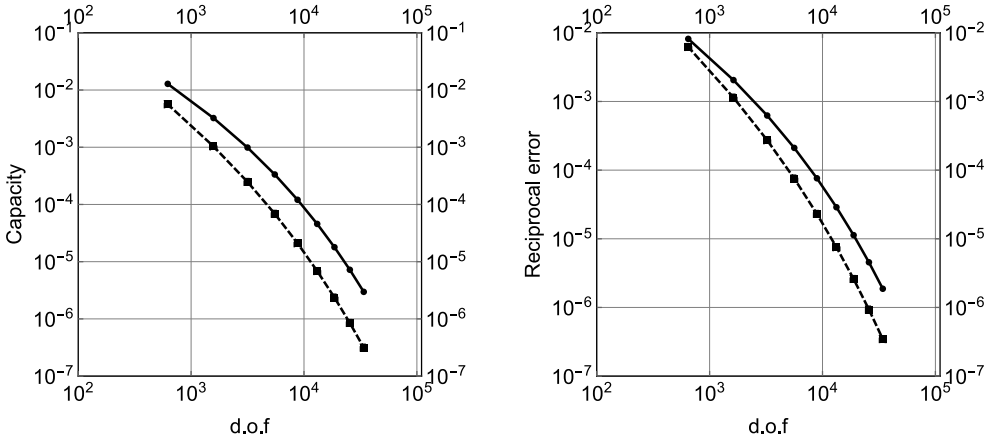

(a) Capacity. (b) Reciprocal error.

Fig. 13. Grötzsch Ring; $R_G(1/2)$. Convergence of capacity and reciprocal error on two circular quadrilaterals. Exact error (solid line); Estimated error (dashed line). Loglog-plots with error vs the number of degrees of freedom. At $p = 10$ the error number = 5.

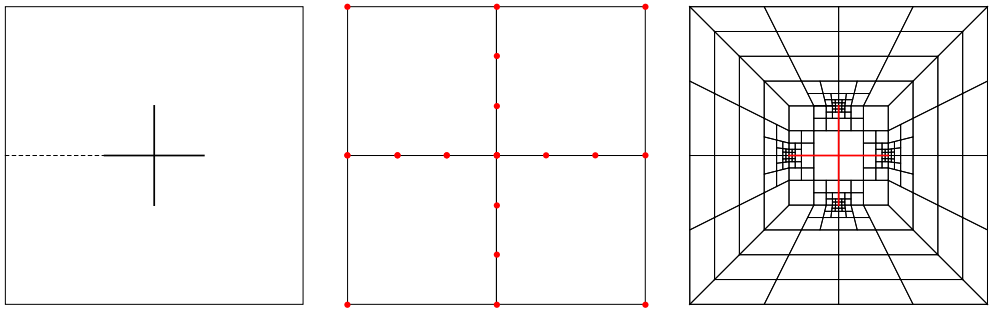

(a) Domain with cut indicated. (b) Four-element configuration. (c) Refined mesh.

(d) Solution of the original problem u_1. (e) Solution of the conjugate problem u_2. (f) Conformal map.

Fig. 14. Planar Capacitor.

In Fig. 14(b) a simple four-element configuration is shown. Since the geometric configuration is aligned with the axis one would expect very good performance and this is indeed confirmed by the convergence graphs of Figs. 15(c) and 15(d). Interestingly the estimate of the reciprocal error overshoots the exact one indicating that the solution of the conjugate problem u_2 in this configuration is not as accurate as u_1. The observed convergence in both cases is exponential, but only just. In the analysis of the results it is important to know that the number of degrees of freedom does not include the inner modes since by definition they are superfluous in this case — every single element is a square.

Please cite this article as: H. Hakula, Adaptive reference elements via harmonic extensions and associated inner modes, Computers and Mathematics with Applications (2020), https://doi.org/10.1016/j.camwa.2020.07.019.

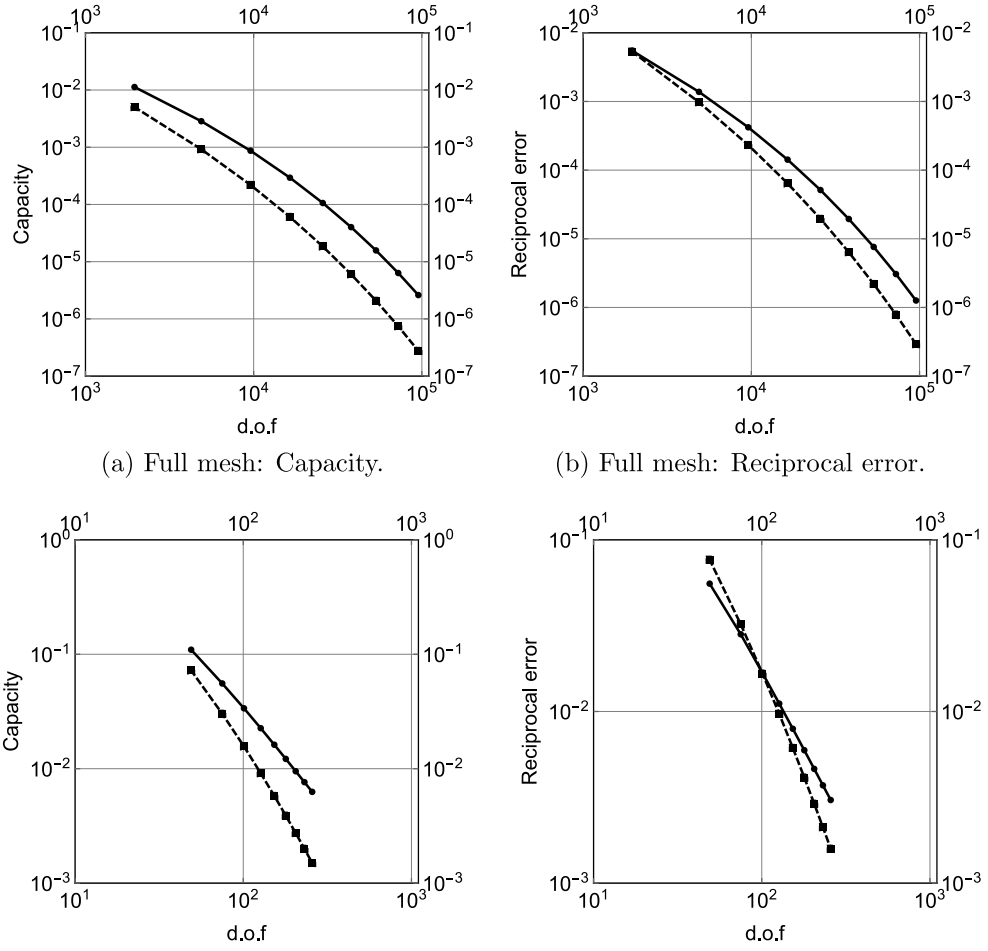

(a) Full mesh: Capacity.

(b) Full mesh: Reciprocal error.

(c) Four-element configuration: Capacity.

(d) Four-element configuration: Reciprocal error.

Fig. 15. Planar Capacitor. Convergence of capacity and reciprocal error on two circular quadrilaterals. Exact error (solid line); Estimated error (dashed line). Loglog-plots with error vs the number of degrees of freedom. In the case of full mesh at $p = 10$ the error number = 5.

4.4. Summary of experiments

In all experiments the expected exponential convergence is observed. Perhaps not surprisingly, the error order is always $= 5$ – the PDE is the same as is the coupling between p and the refinement levels, after all. The error estimate is optimistic and the estimated error order is off by one compared with the true error, and this is reflected in the effectivities as well. Once the reference elements have been computed, the time spent in integration due to element mappings is not significantly higher compared with the standard elements.

5. Conclusions

The proposed non-intrusive extension of the p-version has been inspired by more general approaches on polygonal meshes. Here the admissible elements are those whose underlying reference elements can be mapped with standard mappings. This automatically leads to ambiguity in the sense that for a given set of nodes there are possibly many partitions to mapping and edge (or hanging) nodes.

The numerical experiments indicate that the performance is sufficiently close to p-version. In practice, once the reference elements have been constructed, the higher cost of integration is tolerable. This is an area of future research. Error estimation using FEM constructions is simple to implement. It is not clear yet, how or if at all, the standard approaches such as the auxiliary subspace method should be modified to accommodate the computable shape functions that are not polynomials.

This is the very first paper on this approach. The current implementation is understandably a proof-of-concept, but the numerical experiments show a lot of promise and merit further research.

Please cite this article as: H. Hakula, Adaptive reference elements via harmonic extensions and associated inner modes, Computers and Mathematics with Applications (2020), https://doi.org/10.1016/j.camwa.2020.07.019.

References

[1] L. Beirão da Veiga, F. Brezzi, A. Cangiani, G. Manzini, L.D. Marini, A. Russo, Basic principles of virtual element methods, Math. Models Methods Appl. Sci. 23 (1) (2013) 199—214.
[2] S. Weißer, Arbitrary order Trefftz-like basis functions on polygonal meshes and realization in BEM-based FEM, Comput. Math. Appl. 67 (2014) 1390–1406.
[3] J.S. Ovall, S.E. Reynolds, A high-order method for evaluating derivatives of harmonic functions in planar domains, SIAM J. Sci. Comput. 40 (3) (2018) A1915–A1935.
[4] B. Szabo, I. Babuska, Finite Element Analysis, Wiley, 1991.
[5] C. Schwab, *p*- and *hp*-Finite Element Methods, Oxford University Press, 1998.
[6] P. Solin, K. Segeth, I. Dolezel, Higher-Order Finite Element Methods, Chapman & Hall, 2003.
[7] L. Demkowicz, Computing with *hp*-Adaptive Finite Elements, vol. 1, Chapman & Hall/CRC, 2006.
[8] H. Hakula, M. Neilan, J.S. Ovall, A posteriori estimates using auxiliary subspace techniques, J. Sci. Comput. 72 (1) (2017) 97–127.
[9] E. Burman, S. Claus, P. Hansbo, M.G. Larson, A. Massing, CutFEM: Discretizing geometry and partial differential equations, Internat. J. Numer. Methods Engrg. 104 (7) (2015) 472–501,.
[10] G.D. Anderson, M.K. Vamanamurthy, M. Vuorinen, Conformal Invariants, Inequalities and Quasiconformal Mappings, Wiley-Interscience, 1997.
[11] F.W.J. Olver, D.W. Lozier, R.F. Boisvert, C.W. Clark (Eds.), NIST Handbook of Mathematical Functions, Cambridge, 2010.
[12] H. Hakula, A. Rasila, M. Vuorinen, On moduli of rings and quadrilaterals: algorithms and experiments, SIAM J. Sci. Comput. 33 (2011) 279–302.
[13] H. Hakula, T. Quach, A. Rasila, Conjugate function method for numerical conformal mappings, J. Comput. Appl. Math. 237 (1) (2013) 340–353.
[14] N. Papamichael, N. Stylianopoulos, Numerical Conformal Mapping: Domain Decomposition and the Mapping of Quadrilaterals, World Scientific Publishing Company, 2010.
[15] A.W. Craig, J.Z. Zhu, O.C. Zienkiewicz, A posteriori error estimation, adaptive mesh refinement and multigrid methods using hierarchical finite element bases, in: The Mathematics of Finite Elements and Applications, V (Uxbridge, 1984), Academic Press, London, 1985, pp. 587–594,.
[16] Wolfram Research Inc, Mathematica 12.0, 2019.
[17] H. Hakula, T. Tuominen, Mathematica implementation of the high order finite element method applied to eigenproblems, Computing 95 (1) (2013) 277–301.
[18] P. Hennig, M.A. Osborne, M. Girolami, Probabilistic numerics and uncertainty in computations, Proc. R. Soc. Lond. Ser. A Math. Phys. Eng. Sci. 471 (2015).
[19] H. Hakula, A. Rasila, M. Vuorinen, Conformal modulus and planar domains with strong singularities and cusps, Electron. Trans. Numer. Anal. 48 (2018) 462–478.
[20] S. Bezrodnykh, A. Bogatyrev, S. Goreinov, O. Grigor'ev, H. Hakula, M. Vuorinen, On capacity computation for symmetric polygonal condensers, J. Comput. Appl. Math. 361 (2019) 271–282.

Please cite this article as: H. Hakula, Adaptive reference elements via harmonic extensions and associated inner modes, Computers and Mathematics with Applications (2020), https://doi.org/10.1016/j.camwa.2020.07.019.